Bio-interactions and Biocompatibility

Resolving Bio-Nano Interactions of E.coli Bacteria-Dragonfly Wing Interface with Helium Ion and 3D-Structured Illumination Microscopy to Understand Bacterial Death on Nanotopography

Chaturanga D Bandara, Giulia Ballerin, Miika Leppänen, Tuquabo Tesfamichael, Kostya (Ken) Ostrikov, and Cynthia B. Whitchurch

ACS Biomater. Sci. Eng., **Just Accepted Manuscript** • DOI: 10.1021/acsbiomaterials.9b01973 • Publication Date (Web): 09 Jun 2020

Resolving Bio-Nano Interactions of E. coli Bacteria-Dragonfly Wing Interface with Helium Ion and 3D-Structured Illumination Microscopy to Understand Bacterial Death on Nanotopography

Chaturanga D. Bandara[*†‡], *Giulia Ballerin*[†], *Miika Leppänen*[§], *Tuquabo Tesfamichael*[‡], *Kostya (Ken) Ostrikov*[‡], *and Cynthia B. Whitchurch*[†]

[†]The ithree Institute, University of Technology Sydney, Ultimo, NSW 2007, Australia

[‡]School of Chemistry, Physics and Mechanical Engineering, Science and Engineering Faculty, Queensland University of Technology (QUT), Brisbane, Queensland 4001, Australia

[§]Nanoscience Center, Department of Physics, Department of Biological and Environmental Science, University of Jyvaskyla, FI-40014 Jyvaskyla, Finland

Corresponding Author: chaturangab@yahoo.com

ABSTRACT

Obtaining a comprehensive understanding of the bactericidal mechanisms of natural nanotextured surfaces is crucial for the development of fabricated nanotextured surfaces with efficient bactericidal activity. However, the scale, nature, and speed of bacteria-nanotextured surface interactions make the characterization of the interaction a challenging task. There are currently several different opinions regarding the possible mechanisms by which bacterial membrane damage occurs upon interacting with nanotextured surfaces. Advanced imaging methods could clarify this by enabling visualization of the interaction. Charged particle microscopes can achieve the required nanoscale resolution but are limited to dry samples. In contrast, light-based methods enable the characterization of living (hydrated) samples but are limited by the resolution achievable. Here we utilized both helium ion microscopy (HIM) and 3D structured illumination microscopy (3D-SIM) techniques to understand the interaction of Gram-negative bacterial membranes with nanopillars such as those found on dragonfly wings. Helium ion microscopy enables cutting and imaging at nanoscale resolution while 3D-SIM is a super-resolution optical microscopy technique that allows visualization of live, unfixed bacteria at ~100 nm resolution. Upon bacteria-nanopillar interaction, the energy stored due to the bending of natural nanopillars was estimated and compared with fabricated vertically aligned carbon nanotubes. With the same deflection, shorter dragonfly wing nanopillars store slightly higher energy compared to carbon nanotubes. This indicates that fabricated surfaces may achieve similar bactericidal efficiency as dragonfly wings. This study reports *in situ* characterization of bacteria-nanopillar interactions in real-time close to its natural state. These microscopic approaches will help further understanding of bacterial membrane interactions with nanotextured surfaces and the bactericidal mechanisms of nanotopographies so that more efficient bactericidal nanotextured surfaces can be designed, fabricated, and their bacteria-nanotopography interactions can be assessed *in situ*.

KEYWORDS: bactericidal topography, bio-nano interactions, 3D SIM, dragonfly wing, helium ion microscopy, ion beam milling

INTRODUCTION

The ability of bacteria to adhere, survive and subsequently form biofilms on abiotic surfaces is the leading cause for infection of prostheses after surgery, resulting in implant failure and revision surgery.[1-2] In recent years, there have been significant efforts to reduce infection by developing various nanotextured surfaces on implantable medical devices.[3-4] These nanotextured surfaces are often inspired by nature, and the fabricated topographies are expected to reduce initial bacterial adhesion or kill any bacteria attempting to attach to the surface. The investigation of bacteria-nanotopography interactions has, therefore, become a significant research interest for the efficient and effective development of advanced fabricated bactericidal nanotextured surfaces (NTS) for biomaterials application.[5-8] This is a growing field of research as nanotextured surfaces do not leach bactericidal chemicals, and therefore, the bactericidal property is conserved for longer periods compared to chemical approaches.[9-10] Furthermore, nanotextured surfaces are non-toxic and more effective at controlling bacterial strains that produce extracellular polymeric substance (EPS) secretions.[11-12]

The mechanical bactericidal efficacy of nanotextured surfaces is dependent on the nanotopography, architecture of the nanostructures, surface chemistry, and the type of bacteria.[5, 8, 13-16] However, the antibacterial mechanisms and effectiveness of surface parameters are not well understood due to the limited understanding of the bacteria-nanotopography interactions. Recently, various views and explanations have been proposed for understanding the mechanism of membrane damage.[5-8, 13, 17-21]

Cicada wing-like nanostructures are mainly bactericidal against Gram-negative bacteria.[7, 22-23] The initial report of bacterial membrane damage upon interaction with cicada

wing nanostructures used a differential DNA staining method with confocal microscopy to predict the membrane integrity.[6, 24] This approach is an indirect measurement of the membrane condition, where two separate fluorescent markers are used to stain the nuclear material. As this approach only stains the DNA, it cannot be used to visualize the bacterial membrane directly. Furthermore, due to the limitations in spatial resolution, confocal microscopy can only resolve the color variation of the bacterium and cannot provide detailed information on its membrane integrity. Therefore, to obtain a comprehensive understanding of the effects on the bacterial membrane during the interaction with nanostructures, it would be better to directly visualize the bacterial membrane using super-resolution microscopy techniques such as 3D structured illumination microscopy (3D-SIM) which utilizes spatially patterned fluorescence excitation beams to achieve a resolution of ~100 nm.[25-26]

Recently, the interfaces where bacteria and natural nanotopographies interact have been observed at nanoscale resolution through the use of some of the most advanced microscopic techniques available to-date including helium ion microscopy (HIM), transmission electron microscopy (TEM), focused ion beam (FIB) techniques and faster atomic force microscopy (AFM).[13-14, 17, 27-33] These approaches have furthered our understanding of bacteria-nanotopography interactions of natural surfaces. High-resolution TEM images of cross-sectioned interfaces revealed that the natural nanopillars under the bacteria are bent during the interaction and that dead bacteria appeared to have produced EPS.[13]

A recent study on the interactions of bacteria with Vertically Aligned Carbon Nano Tubes (VACNT) reported the bending of these nanostructures during bacteria-VACNT interactions.[19] This is in line with the previously reported bactericidal effects of natural nanopillar topography of dragonfly wing with *E. coli.*[13] In this study of bacteria-VACNT interactions, the energy stored during bending of multiple lengths of VACNT were quantified, and it was determined that shorter VACNT had more efficient bactericidal activity.[19] The bactericidal mechanisms of

VACNT and black silicon (bSi) have been described in terms of a purely physical mechano-bactericidal basis, and significant differences in the two different surfaces were observed. In bSi, no significant difference in bactericidal activity was reported with changing nanopillar height or its surface chemistry. bSi nanostructure was identified as rigid structures that do not bend when interacting with bacteria.[24] A separate study suggested that adhesion is important but that the membrane is not necessarily pierced by the bSi nanostructures to achieve the bactericidal activity.[14] For VACNT, it was reported that the shorter nanopillars are more efficient and that VACNT bend during interaction with bacteria and in some cases, the bottom surface of bacteria is wrapped by VACNT.[19] Furthermore, when the surface chemistry of VACNT was changed using O_2 or CF_4 plasma, significant changes to bacterial adhesion on the surface and bactericidal activity of *Pseudomonas aeruginosa* were identified.

One plausible mechanism to explain bacterial membrane damage upon interaction with nanopillars is that the bacterial cell first attaches onto the nanopillars, and then while attempting to move parallel to the surface, the nanopillars are bent, and membrane damage occurs through shearing.[13] Another study has suggested that attempted bacterial cell division on the titanium nanotopography causes bacterial membrane damage.[34] When the membrane damage occurs, characteristic EPS production, bending of nanopillars, and leaking of cytoplasm are observed. These post-membrane damage characteristics have recently been observed in HIM, TEM, SEM and confocal studies.[13-14, 17, 19, 28-32, 35] However, as these events occur rapidly, and only at the cell surface, the images obtained using these techniques commonly show the bacteria flattened on the nanopillars, apparently due to membrane damage. It should be noted that the interaction between bacterial membranes and nanostructures cannot be resolved with these microscopic tools due to the limitation in the time-scale or spatial resolution. For instance, extensive sample preparation steps are required prior to imaging the bacteria-nanotopography interaction by TEM, and for FIB, metal deposition is required to reduce charge accumulation for successful

cross-sectioning.[13, 35] As these steps are time-consuming, they prevent capturing the initial stages of the bacterial membrane damage process.

The different observations and interpretations in reports of the mechanobactericidal action of different nanotextured surfaces provide the rationality for further investigations. It remains of urgent and significant importance to evaluate the mechanism of bactericidal activity and bio-nanotopography interactions for both fabricated and natural nanotopographies towards gaining a deeper understanding of the bactericidal mechanism for the efficient design of bactericidal biomaterials.

A combination of approaches could be used to overcome the technical limitations encountered to-date in order to understand the membrane damage process more clearly. One approach would be to freeze the initial stages of bacteria-nanosurface interactions and utilize an imaging technique such as HIM, which has nanoscale resolving power with a larger depth of focus and microscale field of view to image the entire interaction. A second, complementary approach could be to utilize a super-resolution optical imaging technique such as 3D-SIM to image bacteria-nanotopography interactions *in situ* under physiological conditions in real-time. The aim of this work, therefore, was to explore the possibilities of utilizing both HIM and 3D-SIM to provide further insights into *E. coli* bacteria-nanotopography interactions in real-time and thereby further our understanding of the mechanobactericidal activity of the natural nanotopography of dragonfly wings to Gram-negative bacteria. This work supplements previous studies carried out with Gram-negative *Escherichia coli* and dragonfly wings using HIM, AFM, FIB, and TEM.[13, 35] In previous studies, we have used TEM and FIB to expose the interface. Here, we use the Ne^+ beam to cross-section and He^+ to image exposed interface using HIM; thereby, we avoid excessive sample preparation steps associated with TEM and FIB. Special attention is given to the characteristics of the bacteria-nanopillar interface.

RESULTS AND DISCUSSION

Interfacial characteristics of dragonfly wing nanopillars-*Escherichia coli* bacterium by Helium Ion Microscopy (HIM). We used helium ion microscopy (HIM), to examine the bacteria-nanotopography interface of *E. coli* on dragonfly wings. Thin planes of bacteria attached to dragonfly wings were precisely milled using a Ne^+ beam, and the exposed interface imaged using a He^+ beam.[36] This cross-sectioning was carried out without any conductive metal coating, as is required for focused ion beam (FIB) or scanning electron microscopy (SEM).[13, 17] Hence, the bacteria-nanotopography interface images acquired by HIM are not obscured and remain close to their natural state, limiting possible artifacts that might occur during the metal coating processes involved in FIB/SEM. Compared to TEM, this method is flexible for performing cross-sections at various positions, lengths, and directions, whereas TEM is limited to tiny sections of lamellas, and positions of cross-sections cannot be controlled.

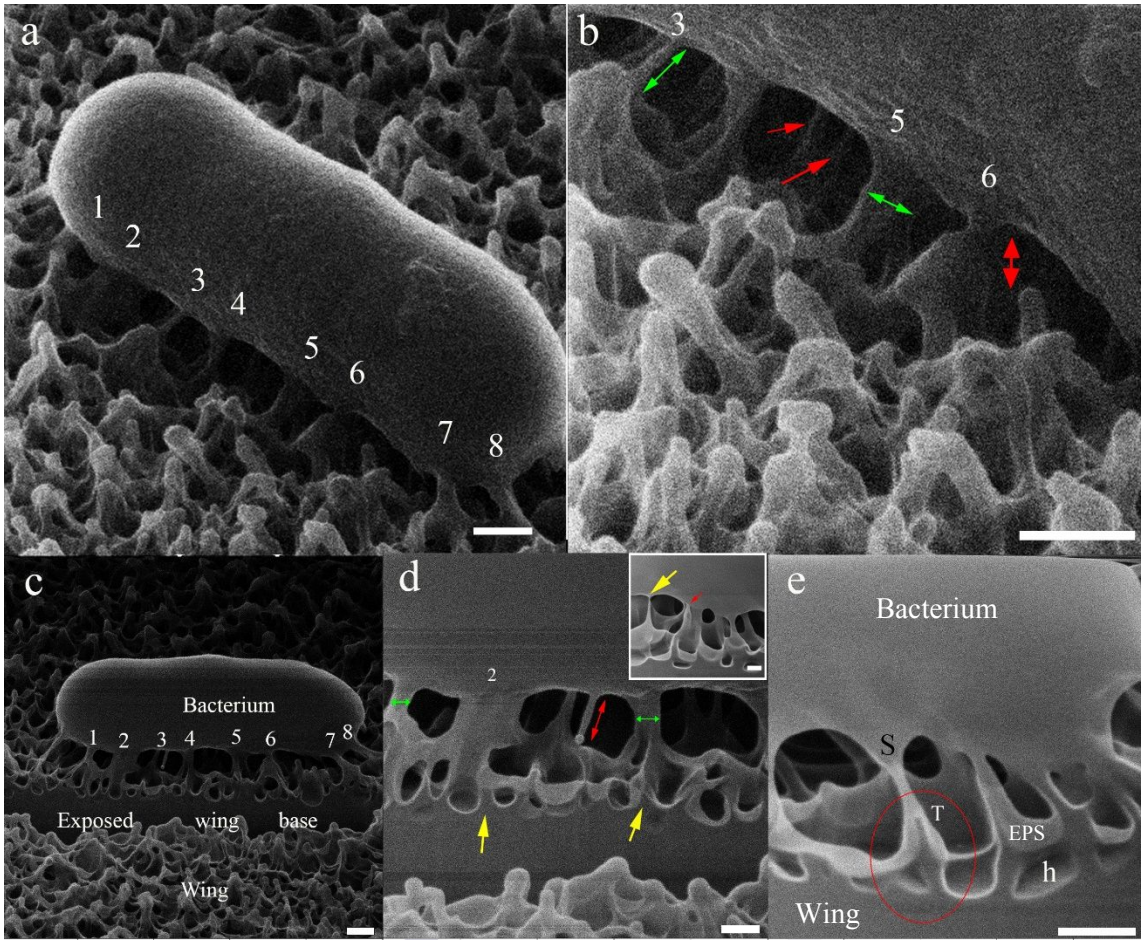

Figure 1: Helium ion beam micrographs are showing initial attachment of bacteria to the nanopillars of dragonfly wings. Panel (a) shows an attached bacterium on to dragonfly wing. Visible connections between the protrusions arising from the bacterium and the nanopillars are numbered for further reference in other panels. b) Magnified region of the bacterium shown in panel (a). The double-headed green arrow represents protrusions that arise from bacterium connecting to the nanopillar on the wing. Red arrows show more connections under the bacterium. The red double-headed arrow shows the gap between a nanopillar and the bacterial membrane. c-e) Interface of *E. coli* bacteria-nanotextured dragonfly wing interface exposed by progressive longitudinal Ne milling. c) Cross-section of the wing and bacteria to expose the interface after approx. 1/3 of the bacterium is removed. Finger-like extensions that connect the bacterium with wing nanopillars are visible. d) Magnified area of (c) and both '2's are the same locations. Visible connection marked 2 is an area where bacterial components heavily flood the underlying nanopillars. Yellow arrows mark the base of nanopillars where the top is flooded by bacterial components. Green-double headed arrows are protrusions connecting bacteria and nanopillars.

The red double-headed arrow shows a finger-like extension from bacteria attaching to nanopillars. Inset shows a magnified area of the interface. A string-like connection is marked by the yellow arrowhead, while a red arrow shows bacterial components flooding. e) The circled area shows a bent nanopillar flooded by a possible EPS secretion, or cytoplasmic content from the bacterium and a partly stretched and deformed membrane marked as 'S.' The tip of the nanopillar is marked T. Holes on the wing are marked h. All scale bars represent 200 nm.

Here, we present the Gram-negative bacteria-natural nanopillar interactions imaged under HIM (Figure 1). *Escherichia coli* cells were incubated for 15 minutes at room temperature on a dragonfly wing and then fixed with 2% glutaraldehyde and subjected to ethanol dehydration before Ne milling and He imaging. This made it possible to image the bacteria-nanotexture interactions before the bacteria are flattened and disintegrate on the nanopillars. The attached bacterium shows multiple connections with the wing via protrusions, some of which are thin and long, while some connections are comparatively thick.

Subsurface details exposed after Ne^+ beam milling of samples are shown in Figure 1c-e. Figure 1c reveals the interface after a longitudinal cross-section was performed at approximately 1/3 of the way across the bacterium and the wing. Here, different connections between the bacterium and the nanostructures are identified and are numbered from 1 to 8 (Figure 1c). These finger-like protrusions connecting the bacterium and the nanotexture are about 100 nm in length and 10-50 nm in diameter. The presence of secreted EPS, cytoplasm, or deformed membrane, finger-like extensions (red double-headed arrow) are visible on the tips of nanopillars (Figure 1d). A red double-headed arrow marks a thin and long extension of material from the bacteria. This suggests that membrane deformations take place at the interface between the bacterial membrane and the nanopillars. The connection numbered 2 in Figure 1d is thicker than the majority of connections identified, which are typically about 100 nm in length and more than 100 nm in thickness. These thick connections could be a

consequence of flooding of the nanopillars by a bacterially-derived substance (Figure 1d), which could be EPS secretions from the bacteria produced upon attachment, leaked cytoplasmic content and/or deformed membrane, indicating membrane damage. The inset (Figure 1d) magnifies a string-like stretch (labeled by a yellow arrow) which starts from the bacterial membrane and floods the top of the adjacent nanopillars. The latter has a thick blanket-like cover that can be identified as a light-colored layer on the wing. Collectively, these visible connections and finger-like protrusions between the bacterium and nanopillars appear to be consistent with the extracellular polymeric substances (EPS) identified in the previous TEM, and SEM/FIB reports.[13] However, at this stage, the composition of this material is not clear and more studies are needed to determine their composition.

The space between the bacterial membrane and nanopillar tips is barely filled by visible connections or finger-like extensions of the bacteria. Most of the nanopillar tips are flooded by bacterial secretions and remain 100-200 nm below the level of the bacterial membrane. Therefore this space is obscured by bacterial secretions. Finger-like connections extending from the bacterial membrane and continuous with nanopillars filling the space, make it difficult to distinguish the bacterial membrane from the nanopillars. Though He ion microscopy is a better technique compared to electron microscopy in contrasting different compositions,[37-41] here, we emphasize that the similar composition of the different components of the sample makes it difficult to distinguish distinct borders of the different components. Nanopillars of the wing are composed of hydrophobic long-chain hydrocarbons[15, 42] while bacterial membranes are comprising of a hydrophobic lipid bilayer and a hydrophilic peptidoglycan layer.[43-44] Therefore, in a favorable chemical environment, interactions between these components may be possible, and a partial or even full encasing of the nanopillars with bacterial membranes could account for the adhesion between Gram-negative bacteria and the nanopillars. Though

we have used a strain without flagella in this study, a one contains flagella would show much favorable interactions with superhydrophobic surfaces.[45]

The circled area of Figure 1e highlights a nanopillar flooded by membrane deformations, EPS, or cytoplasm. The bacterial membrane appears to be extended and stretched towards the nanopillar to form the connection while the nanopillar is slightly tilted or bent to the left from its vertical position. This bending and stretching could be a result of strong adhesion of bacteria and its attempts to move away from the surface.

The above observations and analysis suggest that a series of complex interactions could take place between *E. coli* and natural nanopillar topography before the bacterial membrane is damaged. Therefore, the biological effects of such interactions should also be considered when developing reliable models of the bactericidal effects of antibacterial surfaces.

Further chemical composition studies are required to determine the composition of the finger-like connections we observed between bacteria and nanopillars by HIM. Although we were unable to characterize the nature of the extracellular bacterial-derived substances in this study, at this stage, our approach contributes toward a greater understanding of the bacterial death on nanopillars and will reduce future experimental bias towards just one single bactericidal mechanism.

Interfacial characteristics of dragonfly wing nanopillars-*Escherichia coli* interactions by 3D-SIM. *E. coli* cells were introduced to the wing surface and immediately imaged using 3D-SIM. Cell membranes were pre-stained with the fluorescent lipophilic stain FM1-43 (green) and imaged in the presence of the cell impermeant Ethidium homodimer-III (EthD-III, red) that binds only to the DNA of cells with a compromised membrane. With live 3D-SIM imaging, the dragonfly wing showed faint green auto-fluorescence, whereas the FM1-43-stained bacterial cell membranes show much brighter green fluorescence intensity (Figure 2). Figure

2a shows bacterial cells (arrows) attached to the wing. Membrane damaged bacteria (white arrows) have green membranes and red nuclear DNA (Figure 2a). Figure 2b shows the cross-section of the bacteria-wing interface, where unevenness of the wing is evident. The wing is indicated by a green arrow, and a membrane damaged bacterium by a white arrow. Interestingly, the bacterial cell membrane appears to be missing at the side of the bacterial cell that is in contact with the dragonfly wing (Figure 2a, c). The section views (Figure 2c) clearly show that the bacterial membrane is discontinuous when in contact with the wing surface, thereby allowing the DNA stain EthD-III to enter the cell. Interestingly, we observed that cells that had taken up the dead cell stain (EthD-III) presented different red fluorescence intensities (white arrows, Figure 2a), which suggests that membrane damage may have occurred at different times and/or that different levels of membrane damage have occurred. 3D-SIM utilizes spatially patterned excitation beams to achieve the resolution below the diffraction limit, thereby surpassing the classical spatial resolution limit of conventional microscopy. The 3D-SIM platform used in this study provides a lateral and axial resolution of 110 nm and 280 nm, respectively.[25] By using stains specific for membranes and DNA of membrane-compromised cells, we were able to explore membrane damage in live bacterial cells interacting with dragonfly wings while maintaining physiological conditions. This is the first report of such live *in-situ* imaging of *E. coli* interacting with dragonfly wings with higher contrast between the membrane and nuclear material.

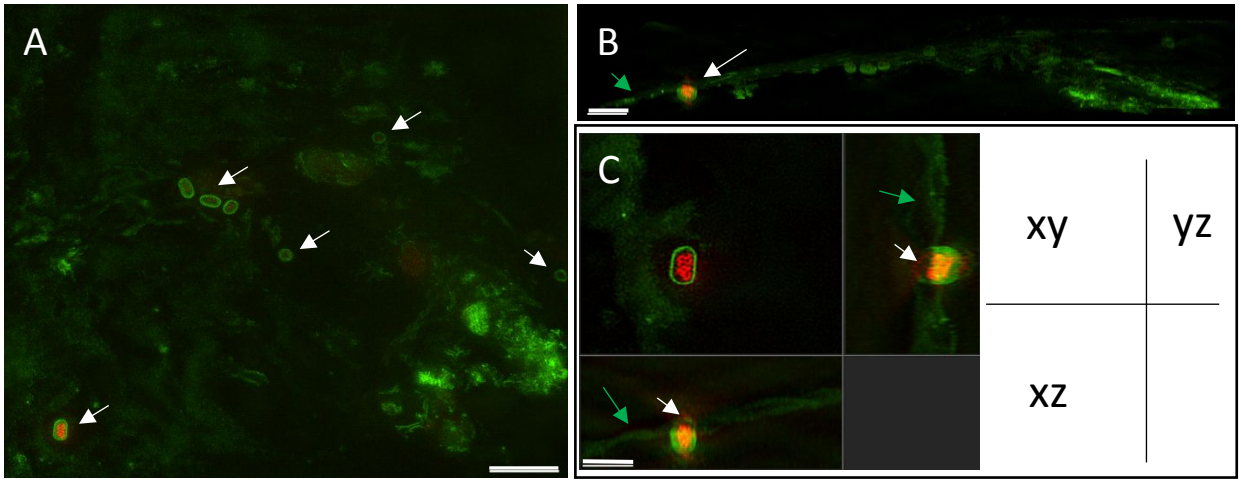

Figure 2: Reconstructed 3D-SIM micrographs showing *E coli* on dragonfly wings A.) Maximum intensity projection showing bacterial cells (white arrows) attached to the wing (green autofluorescence). Scale bar = 5 µm. B.) 3D side view of image A, showing membrane-damaged bacteria (white arrow). The membrane is stained in green and nuclear material stained in red. The green arrow points to the wing. Scale bar = 3 µm. C) Section view of the cell highlighted by the white arrow in image B clearly showing damage (white arrows) at the side of the cell in contact with the dragonfly wing. Scale bar = 2 µm. The graphic shows xy, xz and yz axes for image C.

Elastic energy estimate of bent nanopillars. While our microscopic approach confirms the bending of nanopillars, bacterial membrane stretching, deformation, and damage, microscopy alone do not provide the mechanism that leads to these consequences. The lack of a comprehensive understanding of the bactericidal mechanism ultimately limits the translational potential towards real-world applications of nanotopography. Achieving such knowledge will ultimately lead to the efficient and effective development of real-world applications. A number of recent publications have indicated that the arrangement of nanopillars is not sufficient to achieve the bactericidal activity but that external factors, including the movement of bacteria and bending of nanopillars, also contribute to the bactericidal activity of dragonfly nanopillars.[21, 46]

To assess the contribution of bending of dragonfly nanopillars on the underlying mechanism of bactericidal activity, we estimated the amounts of the stored elastic energies of natural nanotopography of dragonfly wings during interactions with bacteria. This data could then be used to design artificial bactericidal surfaces and compare them with fabricated nanopillars. As we have identified that bending of dragonfly wing nanopillars occurs when the bacterial membrane is being damaged,[13] we assessed the storage of energy in the bending of dragonfly nanopillars. According to the model suggested by Linklater *et al.*[19] for a surface with VACNT, using Bernoulli's beam theory, a force, P (load) acting on the tip of a nanopillar parallel to the substratum when a bacterium attempts to move, predicts a deflection of the tip, δ as;

$$\delta = \frac{PL^3}{3\,EI} \qquad (1)$$

where L is the length of the nanopillar, E is the material's Young modulus, and I the area moment.

According to Eq. (1), the deflection is much bigger in a longer nanopillar. On the other hand, the elastic energy stored, $U = \frac{3EI\delta^2}{2L^3}$, can be balanced by the external energy, $W = \frac{P\delta}{2}$. Thus, for a constant deflection (δ) of the nanopillar, the elastic energy (U) is proportional to the Young's modulus (E) and inversely related to L^3. That means, for a given deflection, longer nanopillars stores smaller energy.

According to these storage energy calculations, both dragonfly wing nanopillars and 1 μm CNT store similar energies upon the same tip deflection (Figure 3). With the same tip displacement, short nanopillars of the dragonfly wing exert stronger forces than tall nanopillars, while 1 μm VACNT energy storage values are in between short and tall nanopillars. Consequently, the natural nanotopography of dragonfly wings may induce more damage to the bacterial cell membrane than CNT.

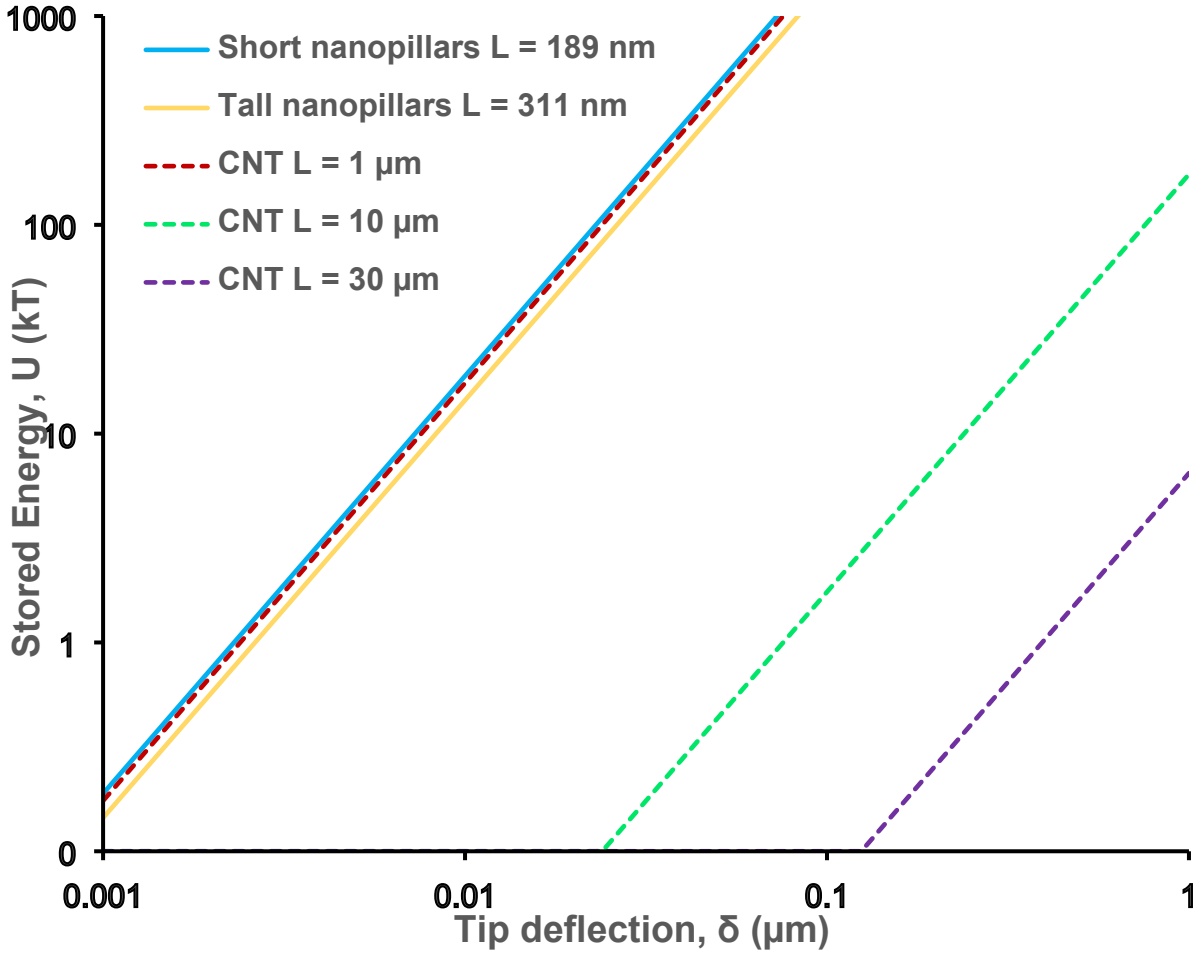

Figure 3: The stored energy comparison in CNT and in dragonfly nanopillars against tip deflection. Shorter and taller dragonfly wing nanopillars store energies similar to those stored in 1 µm CNT. Dragonfly wing data are plotted as solid lines, and CNT data are plotted as dotted lines. 1 kT at 298 K corresponds to 4.11 x 10^{-21} J. *Data reproduced with permission from "Linklater et al, ACS Nano 2018, 12, 7, 6657-6667, DOI: 10.1021/acsnano.8b01665 copyright © 2018, American Chemical Society.*

We observed with HIM that the interacting nanopillars with bacteria are bent, maybe when bacterium attempts to move. The stored energy due to bending of the nanopillars may release, leading to further stretching of the bacterial membrane causing physical damage to the membrane.

CONCLUSIONS

To address the challenges of characterizing the interface of bacterial cells and biological nanotopographies and interpreting the mechanical basis of bactericidal activities, we have designed an approach to examine the nano-biointerface close to its natural state. This unique approach has highlighted several key characteristics that have important implications for the design of efficient and effective nanotextured surfaces for biomedical applications.

This study has utilized sophisticated imaging techniques with minimal sample processing that has important implications for the comprehensive understanding of the biointerface. By using a Ne^+ beam and electron flood gun, we eliminated the use of a conductive metal coating that is used in SEM and avoids the application of metal layer onto the sample prior to cross-sectioning, as reported previously in FIB/SEM and TEM studies.[13, 17, 19, 27] Elimination of both metal coating and Pt deposition allowed us to image the bacteria-nanopillar interaction close to its natural state. Ne^+ beam cross-sectioning has allowed us to cross-section small amounts of the sample at specific positions, where TEM cross-sections are random. This has allowed us to observe the interfacial features, at precise locations with more clarity and without disturbance at nanoscale resolution. In *E. coli*, it was found that bacteria and nanopillars make contacts at specific anchor locations. Finger-like protrusions, possible secreted EPS, cytoplasmic material, and membrane deformations were also visible; however, they were not able to be distinguished using ion beam microscopy. Further, it was confirmed that the membrane is not pierced by the nanopillars, but is more likely stretched and deformed during the interaction.

With live 3D-SIM, bacterial membranes and the nuclear material of membrane-compromised cells were resolved. However, the nanopillars or finger-like protrusions that we observed with HIM could not be visualized with 3D-SIM due to the resolution limit of this technique. We were, however, able to observe that membrane damage occurred at the surface of the bacterial

cell that was in contact with the dragonfly wing. Although neither of the imaging methods alone could fully resolve the interactions between the nanopillar and the bacteria, this study provides useful insight into the limits and possibilities of the imaging methods. It is evident from this study that multiple experimental approaches that involve minimal sample processing are necessary to comprehensively assess the bactericidal activity of nanotextured surfaces.

Further mechanical insights were obtained by estimating the bending energy storage of short and tall nanopillars of the dragonfly wings. These elastic energy storage estimations indicated that short nanopillars are slightly higher in energy storage compared to tall nanopillars of the dragonfly wing. It was also found that 1 μm VACNT energy storage is between that of the tall and short nanopillars of dragonfly wings. This indicates that both natural bactericidal nanotopography and VACNT are likely to mechanically behave quite similarly in achieving bactericidal activity. This suggests that soft materials can achieve bactericidal effects and that antibacterial surfaces do not necessarily need to be designed using hard solid materials.

The microscopy techniques that we utilized in this study distinguished the features of the interface between a Gram-negative bacterium and the dragonfly wing. Given that Gram-negative and Gram-positive bacteria have significant differences in their cell wall and membrane structures, in future studies, bacterial surface/nanotopography interfaces should be examined with techniques capable of nanoscale and molecular resolution with minimal processing. Our approach could be applied to examine interactions of Gram-positive and Gram-negative bacteria and eukaryotic cells with various nanotopographies to guide the design of efficient nanofabrication.

EXPERIMENTAL SECTION

Dragonfly wing collection and sample preparation. The dragonfly specimens were collected in Brisbane, Australia and wings were aseptically removed from the body, washed with flowing deionized water, and stored in the dark at 4°C in sterile containers.

Bacterial growth conditions and sample preparation for HIM. The *Escherichia coli* (NCTC 10418) strain was used for the HIM study. Bacterial cultures were grown overnight at 37 ^{o}C in 5 mL of nutrient broth. The culture was collected at the logarithmic stage of growth, and the bacteria suspension was washed twice with 0.01 M PBS (pH=7.4) and adjusted to OD_{600}=0.3. A 200 µL aliquot of bacterial suspension was placed on a 5 mm x 5 mm size wing and allowed to incubate at room temperature (22^{o}C) in a Petri dish.[13, 27] Wings were then gently washed with sterile MiliQ water to remove non-attached cells.

Ne^+ milling and He^+ imaging of interface with Helium Ion Microscope. For Ne^+ milling, *E. coli* cells incubated for 15 minutes on a dragonfly wing was used. Samples were fixed with 2% glutaraldehyde and subjected to membrane staining and ethanol dehydration.[13, 27] Dehydrated and dried wings were mounted using double-sided carbon tape onto an aluminum stab for imaging. Zeiss Orion NanoFab equipped with Ne^+ and He^+ beam was used for cross-sectioning of bacterial cells attached to the dragonfly wing. Samples were not coated, and no other depositions were performed before imaging/milling. Bacteria were cross-sectioned in longitudinal direction progressively and micrographed after each cross-section so that interactions can be studied. Milling was performed with and Ne^+ at an acceleration voltage of 15 kV. Ion current varied between 4-10 pA during the milling, and pixel dwell time was set to 2-5 µs. Milling was done from the 50 degrees tilted angle by drawing the reduced raster scan rectangle over the area to be removed and waiting until the material disappeared. The sample was then rotated and imaged with He^+. When imaging, 30 kV acceleration voltage and 0.2-0.4 pA ion current were used with line averages of 16 or 32 and dwell time 0.5 or 1 µs. During

both milling and imaging, flood gun charge compensation was used. For a single dragonfly wing sample, 3-5 wing cells were analyzed. A cell of a dragonfly wing is the membranous area that is enclosed by the veins. We have analyzed at least 3 bacterial cells within a single cell of a wing, which makes about 10 cells per sample. We have carried out experiments in duplicate.

Bacterial growth conditions and sample preparation for 3D-SIM microscopy. *E. coli* MG1655 was cultured in LB media at 37 ºC overnight with vigorous shaking. 500 µL of the overnight culture was harvested by centrifugation at 9000 rpm for 1.5 min and re-suspended in 500 µL of PBS. The bacterial suspension was stained with FM1-43FX (Life Technologies) at 4 µg/mL for 15 minutes. The bacterial suspension was then washed twice in PBS and re-suspended in 500 µL of PBS. A small piece of dragonfly wing (5 x 5 mm) was immersed in the membrane-stained bacterial suspension for about 30 min to allow bacteria attachment on the wing. The wing was then carefully removed from the solution and washed in 500 µL of PBS to remove non-adherent bacterial cells. The wing was then immersed in 500 µL of PBS containing Ethidium homodimer-III (Biotium) at 1 µM and stained for 15 min. The wing was then immersed in 500 µL of fresh PBS to wash dye excess. An adhesive frame (Gene Frame®, Thermo Fisher Scientific) was placed on a microscope slide to create a chamber, the wing was attached inside the chamber using a UV glue (Dymax), and PBS was used as mounting media for imaging. A #1.5, 22x22 mm glass coverslip was ethanol sterilized and placed on top.

3D-Structured Illumination Microscopy (3D-SIM). Samples were immediately imaged using the DeltaVision OMX-SR (GE Healthcare) platform at 37 ºC with a 60x oil objective. 3D images were acquired with a z-step size of 0.125 µm for 3 µm total thickness. Raw images were processed with SoftWoRx (GE Healthcare) for image reconstruction and channel alignment and then prepared with IMARIS (v 9.1.2, Bitplane).

AUTHOR INFORMATION

Corresponding Author

chaturangab@yahoo.com

ORCID

Chaturanga D. Bandara 0000-0002-0688-4260

Giulia Ballerin 0000-0001-9551-7405

Miika Leppänen 0000-0002-1855-8390

Tuquabo Tesfamichael 0000-0001-7012-4904

Kostya (Ken) Ostrikov 0000-0001-8672-9297

Cynthia Whitchurch 0000-0003-2296-3791

Author contributions

C.D.B. initiated the project, prepared the samples, performed cell viability tests, HIM imaging and wrote the manuscript. M.L. performed HIM milling and imaging of bacteria. G.B. performed 3D-SIM imaging. All authors contributed to the data analysis, results interpretation, manuscript preparation, and approved the final version.

Notes

The authors declare no competing financial interest.

ACKNOWLEDGEMENTS

Work of Miika Leppänen was supported by the Jane and Aatos Erkko Foundation. Work of Chaturanga Bandara was partly supported by SEF Write-up scholarship. Authors acknowledge Facilities of Central Analytical Research Facility (CARF, IFE) at Queensland University of Technology and ithree Institute at University of Technology Sydney.

REFERENCES

1. Berne, C.; Ducret, A.; Hardy, G. G.; Brun, Y. V., Adhesins involved in attachment to abiotic surfaces by Gram-negative bacteria. *Microbiology spectrum* **2015,** *3* (4), 10.1128/microbiolspec.MB-0018-2015. DOI: 10.1128/microbiolspec.MB-0018-2015.
2. Petrova, O. E.; Sauer, K., Sticky Situations: Key Components That Control Bacterial Surface Attachment. *J. Bacteriol.* **2012,** *194* (10), 2413-2425. DOI: 10.1128/jb.00003-12.
3. Nejadnik, M. R.; van der Mei, H. C.; Norde, W.; Busscher, H. J., Bacterial adhesion and growth on a polymer brush-coating. *Biomaterials* **2008,** *29* (30), 4117-4121. DOI: 10.1016/j.biomaterials.2008.07.014.
4. Harris, L.; Meredith, D. O.; Eschbach, L.; Richards, R. G., Staphylococcus aureus adhesion to standard micro-rough and electropolished implant materials. *J. Mater. Sci. Mater. Med.* **2007,** *18* (6), 1151-1156. DOI: 10.1007/s10856-007-0143-0.
5. Watson, G. S.; Green, D. W.; Watson, J. A.; Zhou, Z.; Li, X.; Cheung, G. S. P.; Gellender, M., A Simple Model for Binding and Rupture of Bacterial Cells on Nanopillar Surfaces. *Advanced Materials Interfaces* **2019**, 1801646. DOI: 10.1002/admi.201801646.
6. Pogodin, S.; Hasan, J.; Baulin, V. A.; Webb, H. K.; Truong, V. K.; Phong Nguyen, T. H.; Boshkovikj, V.; Fluke, C. J.; Watson, G. S.; Watson, J. A.; Crawford, R. J.; Ivanova, E. P., Biophysical model of bacterial cell interactions with nanopatterned cicada wing surfaces. *Biophys. J.* **2013,** *104* (4), 835-840.
7. Ivanova, E. P.; Hasan, J.; Webb, H. K.; Truong, V. K.; Watson, G. S.; Watson, J. A.; Baulin, V. A.; Pogodin, S.; Wang, J. Y.; Tobin, M. J.; Löbbe, C.; Crawford, R. J., Natural bactericidal surfaces: Mechanical rupture of pseudomonas aeruginosa cells by cicada wings. *Small* **2012,** *8* (16), 2489-2494.
8. Liu, T.; Cui, Q.; Wu, Q.; Li, X.; Song, K.; Ge, D.; Guan, S., Mechanism Study of Bacteria Killed on Nanostructures. *J. Phys. Chem. B* **2019,** *123* (41), 8686-8696. DOI: 10.1021/acs.jpcb.9b07732.
9. AshaRani, P. V.; Low Kah Mun, G.; Hande, M. P.; Valiyaveettil, S., Cytotoxicity and Genotoxicity of Silver Nanoparticles in Human Cells. *ACS Nano* **2009,** *3* (2), 279 - 290. DOI: 10.1021/nn800596w.
10. Gatti, A. M.; Montanari, S.; Gambarelli, A.; Capitani, F.; Salvatori, R., In-vivo short- and long-term evaluation of the interaction material-blood. *J. Mater. Sci. Mater. Med.* **2005,** *16* (12), 1213-9. DOI: 10.1007/s10856-005-4731-6.
11. Das, B.; Khan, M. I.; Jayabalan, R.; Behera, S. K.; Yun, S. I.; Tripathy, S. K.; Mishra, A., Understanding the Antifungal Mechanism of Ag@ZnO Core-shell Nanocomposites against Candida krusei. *Sci. Rep.* **2016,** *6*, 36403. DOI: 10.1038/srep36403.
12. Kruszewski, K. M.; Nistico, L.; Longwell, M. J.; Hynes, M. J.; Maurer, J. A.; Hall-Stoodley, L.; Gawalt, E. S., Reducing Staphylococcus aureus biofilm formation on stainless steel 316L using functionalized self-assembled monolayers. *Materials Science and Engineering: C* **2013,** *33* (4), 2059-2069. DOI: http://dx.doi.org/10.1016/j.msec.2013.01.023.
13. Bandara, C. D.; Singh, S.; Afara, I. O.; Tesfamichael, T.; Wolff, A.; Ostrikov, K.; Oloyede, A., Bactericidal Effects of Natural Nanotopography of Dragonfly Wing on Escherichia coli. *ACS Applied Materials & Interfaces* **2017,** *9* (8), 6746-6760. DOI: 10.1021/acsami.6b13666.
14. Michalska, M.; Gambacorta, F.; Divan, R.; Aranson, I. S.; Sokolov, A.; Noirot, P.; Laible, P. D., Tuning antimicrobial properties of biomimetic nanopatterned surfaces. *Nanoscale* **2018,** *10* (14), 6639-6650. DOI: 10.1039/C8NR00439K.
15. Román-Kustas, J.; Hoffman, J. B.; Reed, J. H.; Gonsalves, A. E.; Oh, J.; Li, L.; Hong, S.; Jo, K. D.; Dana, C. E.; Miljkovic, N.; Cropek, D. M.; Alleyne, M., Molecular and Topographical Organization: Influence on Cicada Wing Wettability and Bactericidal Properties. *Advanced Materials Interfaces* **2020**, 2000112. DOI: 10.1002/admi.202000112.
16. Ziegler, N.; Sengstock, C.; Mai, V.; Schildhauer, T. A.; Koller, M.; Ludwig, A., Glancing-Angle Deposition of Nanostructures on an Implant Material Surface. *Nanomaterials (Basel)* **2019,** *9* (1). DOI: 10.3390/nano9010060.

17. Linklater, D. P.; Juodkazis, S.; Rubanov, S.; Ivanova, E. P., Comment on "Bactericidal Effects of Natural Nanotopography of Dragonfly Wing on Escherichia coli". *ACS Applied Materials & Interfaces* **2017,** *9* (35), 29387-29393. DOI: 10.1021/acsami.7b05707.
18. Xue, F.; Liu, J.; Guo, L.; Zhang, L.; Li, Q., Theoretical study on the bactericidal nature of nanopatterned surfaces. *J. Theor. Biol.* **2015,** *385*, 1-7. DOI: 10.1016/j.jtbi.2015.08.011.
19. Linklater, D. P.; De Volder, M.; Baulin, V. A.; Werner, M.; Jessl, S.; Golozar, M.; Maggini, L.; Rubanov, S.; Hanssen, E.; Juodkazis, S.; Ivanova, E. P., High Aspect Ratio Nanostructures Kill Bacteria via Storage and Release of Mechanical Energy. *ACS Nano* **2018,** *12* (7), 6657-6667. DOI: 10.1021/acsnano.8b01665.
20. Jenkins, J.; Mantell, J.; Neal, C.; Gholinia, A.; Verkade, P.; Nobbs, A. H.; Su, B., Antibacterial effects of nanopillar surfaces are mediated by cell impedance, penetration and induction of oxidative stress. *Nature Communications* **2020,** *11* (1), 1626. DOI: 10.1038/s41467-020-15471-x.
21. Valiei, A.; Lin, N.; Bryche, J.-F.; McKay, G.; Canva, M.; Charette, P. G.; Nguyen, D.; Moraes, C.; Tufenkji, N., Mechano-bactericidal nanopillars require external forces to effectively kill bacteria. *bioRxiv* **2020**, 2020.03.27.012153. DOI: 10.1101/2020.03.27.012153.
22. Hasan, J.; Crawford, R. J.; Ivanova, E. P., Antibacterial surfaces: the quest for a new generation of biomaterials. *Trends Biotechnol.* **2013,** *31* (5), 295-304. DOI: 10.1016/j.tibtech.2013.01.017.
23. Hasan, J.; Webb, H. K.; Truong, V. K.; Pogodin, S.; Baulin, V. A.; Watson, G. S.; Watson, J. A.; Crawford, R. J.; Ivanova, E. P., Selective bactericidal activity of nanopatterned superhydrophobic cicada Psaltoda claripennis wing surfaces. *Appl. Microbiol. Biotechnol.* **2012,** *97* (20), 1-6. DOI: 10.1007/s00253-012-4628-5.
24. Ivanova, E. P.; Hasan, J.; Webb, H. K.; Gervinskas, G.; Juodkazis, S.; Truong, V. K.; Wu, A. H.; Lamb, R. N.; Baulin, V. A.; Watson, G. S.; Watson, J. A.; Mainwaring, D. E.; Crawford, R. J., Bactericidal activity of black silicon. *Nat Commun* **2013,** *4*, 2838. DOI: http://dx.doi.org/10.1038/ncomms3838.
25. Huang, B.; Bates, M.; Zhuang, X., Super-Resolution Fluorescence Microscopy. *Annu. Rev. Biochem.* **2009,** *78* (1), 993-1016. DOI: 10.1146/annurev.biochem.77.061906.092014.
26. Turnbull, L.; Toyofuku, M.; Hynen, A. L.; Kurosawa, M.; Pessi, G.; Petty, N. K.; Osvath, S. R.; Cárcamo-Oyarce, G.; Gloag, E. S.; Shimoni, R.; Omasits, U.; Ito, S.; Yap, X.; Monahan, L. G.; Cavaliere, R.; Ahrens, C. H.; Charles, I. G.; Nomura, N.; Eberl, L.; Whitchurch, C. B., Explosive cell lysis as a mechanism for the biogenesis of bacterial membrane vesicles and biofilms. *Nature communications* **2016,** *7*, 11220-11220. DOI: 10.1038/ncomms11220.
27. Imihami Mudiyanselage, C. C. D. B. Characterisation of the bactericidal efficacy of natural nano-topography using dragonfly wing as a model. Ph.D. Dissertation, Queensland University of Technology, Brisbane, QLD, 2017. DOI: 10.5204/thesis.eprints.106746.
28. Oh, Y. J.; Khan, E. S.; Campo, A. d.; Hinterdorfer, P.; Li, B., Nanoscale Characteristics and Antimicrobial Properties of (SI-ATRP)-Seeded Polymer Brush Surfaces. *ACS Applied Materials & Interfaces* **2019,** *11* (32), 29312-29319. DOI: 10.1021/acsami.9b09885.
29. Reed, J. H.; Gonsalves, A. E.; Román, J. K.; Oh, J.; Cha, H.; Dana, C. E.; Toc, M.; Hong, S.; Hoffman, J. B.; Andrade, J. E.; Jo, K. D.; Alleyne, M.; Miljkovic, N.; Cropek, D. M., Ultrascalable Multifunctional Nanoengineered Copper and Aluminum for Antiadhesion and Bactericidal Applications. *ACS Applied Bio Materials* **2019,** *2* (7), 2726-2737. DOI: 10.1021/acsabm.8b00765.
30. Nakade, K.; Jindai, K.; Sagawa, T.; Kojima, H.; Shimizu, T.; Shingubara, S.; Ito, T., Adhesion and Bactericidal Properties of a Wettability-Controlled Artificial Nanostructure. *ACS Applied Nano Materials* **2018,** *1* (10), 5736-5741. DOI: 10.1021/acsanm.8b01340.
31. Boinovich, L. B.; Modin, E. B.; Aleshkin, A. V.; Emelyanenko, K. A.; Zulkarneev, E. R.; Kiseleva, I. A.; Vasiliev, A. L.; Emelyanenko, A. M., Effective Antibacterial Nanotextured Surfaces Based on Extreme Wettability and Bacteriophage Seeding. *ACS Applied Nano Materials* **2018,** *1* (3), 1348-1359. DOI: 10.1021/acsanm.8b00090.
32. Ito, T.; Nakade, K.; Jindai, K.; Sagawa, T.; Kojima, H.; Shimizu, T.; Shingubara, S., *Time-lapse imaging of bactericidal effect on nanostructural surface*. SPIE: 2019; Vol. 10965.

33. Banner, D. J.; Firlar, E.; Jakubonis, J.; Baggia, Y.; Osborn, J. K.; Shahbazian-Yassar, R.; Megaridis, C. M.; Shokuhfar, T., Correlative ex situ and Liquid-Cell TEM Observation of Bacterial Cell Membrane Damage Induced by Rough Surface Topology. *Int J Nanomedicine* **2020,** *15* (15), 1929-1938. DOI: 10.2147/IJN.S232230.
34. Köller, M.; Ziegler, N.; Sengstock, C.; Schildhauer, T. A.; Ludwig, A., Bacterial cell division is involved in the damage of gram-negative bacteria on a nano-pillar titanium surface. *Biomedical Physics & Engineering Express* **2018,** *4* (5), 055002. DOI: 10.1088/2057-1976/aad2c1.
35. Imihami Mudiyanselage, C. C. D. B. Characterisation of the bactericidal efficacy of natural nano-topography using dragonfly wing as a model. PhD, 2017. DOI: 10.5204/thesis.eprints.106746.
36. Leppänen, M., Imaging Bacterial Colonies and Phage-bacterium Interaction at Sub-nanometer Resolution Using Helium Ion Microscopy. 2017.
37. Bell, D., Contrast Performance: Low Voltage Electrons vs. Helium Ions. *Microsc. Microanal.* **2011,** *17* (SupplementS2), 660-661. DOI: doi:10.1017/S143192761100417X.
38. Joy, D. C., Helium Ion Microscopy : Principles and Applications. 1 ed.; Springer: Dordrecht, 2013. http://QUT.eblib.com.au/patron/FullRecord.aspx?p=1466751.
39. Boseman, A.; Nowlin, K.; Ashraf, S.; Yang, J.; LaJeunesse, D., Ultrastructural analysis of wild type and mutant Drosophila melanogaster using helium ion microscopy. *Micron* **2013,** *51*, 26-35. DOI: http://dx.doi.org/10.1016/j.micron.2013.06.005.
40. Joens, M. S.; Huynh, C.; Kasuboski, J. M.; Ferranti, D.; Sigal, Y. J.; Zeitvogel, F.; Obst, M.; Burkhardt, C. J.; Curran, K. P.; Chalasani, S. H.; Stern, L. A.; Goetze, B.; Fitzpatrick, J. A. J., Helium Ion Microscopy (HIM) for the imaging of biological samples at sub-nanometer resolution. *Sci. Rep.* **2013,** *3*, 3514. DOI: 10.1038/srep03514.
41. Ki Woo, K., Biological Applications of Helium Ion Microscopy. *Applied Microscopy* **2013,** *43* (1), 9-13.
42. Ivanova, E. P.; Nguyen, S. H.; Webb, H. K.; Hasan, J.; Truong, V. K.; Lamb, R. N.; Duan, X.; Tobin, M. J.; Mahon, P. J.; Crawford, R. J., Molecular Organization of the Nanoscale Surface Structures of the Dragonfly *Hemianax papuensis* Wing Epicuticle. *PLoS One* **2013,** *8* (7), e67893. DOI: 10.1371/journal.pone.0067893.
43. Tortora, G. J.; Funke, B. R.; Case, C. L., *Microbiology an introduction*. 10 ed.; Pearson Education Inc.: San Francisco, CA 94111, 2010.
44. Vollmer, W.; Seligman, S. J., Architecture of peptidoglycan: more data and more models. *Trends Microbiol.* **2010,** *18* (2), 59-66. DOI: http://dx.doi.org/10.1016/j.tim.2009.12.004.
45. Friedlander, R. S.; Vogel, N.; Aizenberg, J., Role of Flagella in Adhesion of Escherichia coli to Abiotic Surfaces. *Langmuir* **2015,** *31* (22), 6137-6144. DOI: 10.1021/acs.langmuir.5b00815.
46. Jindai, K.; Nakade, K.; Masuda, K.; Sagawa, T.; Kojima, H.; Shimizu, T.; Shingubara, S.; Ito, T., Adhesion and bactericidal properties of nanostructured surfaces dependent on bacterial motility. *RSC Advances* **2020,** *10* (10), 5673-5680. DOI: 10.1039/C9RA08282D.

Resolving Bio-Nano Interactions of E. coli Bacteria-Dragonfly Wing Interface with Helium Ion and 3D-Structured Illumination Microscopy to Understand Bacterial Death on Nanotopography

Chaturanga D. Bandara[*†‡], *Giulia Ballerin*[†], *Miika Leppänen*[§], *Tuquabo Tesfamichael*[‡], *Kostya (Ken) Ostrikov*[‡], *and Cynthia B. Whitchurch*[†]

[†]The ithree Institute, University of Technology Sydney, Ultimo, NSW 2007, Australia

[‡]School of Chemistry, Physics and Mechanical Engineering, Science and Engineering Faculty, Queensland University of Technology (QUT), Brisbane, Queensland 4001, Australia

[§]Nanoscience Center, Department of Physics, Department of Biological and Environmental Science, University of Jyvaskyla, FI-40014 Jyvaskyla, Finland

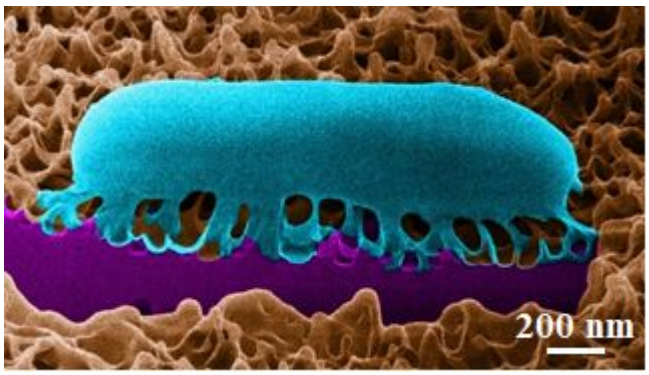

TOC Figure